Environmental Photochemistry of Nitro-PAHs: Direct Observation of Ultrafast Intersystem Crossing in 1-Nitropyrene

Carlos E. Crespo-Hernández,*,† Gotard Burdzinski,‡ and Rafael Arce§

Center for Chemical Dynamics, Department of Chemistry, Case Western Reserve University, 10900 Euclid Avenue, Cleveland, Ohio 44106, Quantum Electronics Laboratory, Faculty of Physics, Adam Mickiewicz University, 85 Umultowska, Poznan 61-614, Poland, and Department of Chemistry, University of Puerto Rico, San Juan Campus, San Juan, Puerto Rico 00936

Received: March 17, 2008

Femtosecond broadband transient absorption experiments of 1-nitropyrene, a nitro-polycyclic aromatic hydrocarbon of environmental concern are presented in cyclohexane and hexane solutions. The transient absorption spectra show the presence of three species that are assigned to the Franck−Condon excited lowest singlet (S_1) state, the structurally relaxed S_1 state, and the lowest excited triplet state. The spectral changes at early times are interpreted in terms of conformational dynamics; primarily due to an ultrafast rotation of the nitro group in the S_1 state. This excited state relaxation is followed by intersystem crossing with a time constant of 7 ps. CIS/6-31G(d,p) calculations predict planarization of the nitro-aromatic torsional angle as the major nuclear relaxation coordinate, from 32.8° at the HF/6-31G(d,p) level of theory in the ground state (27.46° at B3LYP/6-31++G(d,p)) to 0.07° in the S_1 state. Vertical excitation energies at the TDDFT/6-31++G(d,p) and TDDFT/IEFPCM/6-31++G(d,p) levels of theory predict a small energy gap (<0.12 eV) between the $S_1(\pi\pi^*)$ state and the third excited triplet state $T_3(n\pi^*)$ in the gas phase and in cyclohexane, respectively. The small energy gap suggests a large spin-orbit coupling between the $S_1(\pi\pi^*)$ and $T_3(n\pi^*)$ states, which explains the ultrafast intersystem crossing of 1-nitropyrene in nonpolar solvents.

Introduction

Nitro-polycyclic aromatic hydrocarbons (nitro-PAHs) constitute one of the most important classes of environmental pollutants, found in air, aquatic systems, grilled food, and sediments.[1–6] Nitro-PAHs are released to the environment as a result of direct emissions from incomplete combustion processes[7,8] and are formed in situ in the atmosphere by gas phase oxidation and nitrite (NO_3) radical reactions of PAHs.[9–11] Many nitro-PAHs have been identified as mutagenic and carcinogenic agents, and continued concern about these compounds derives from the potential risk they pose to human health.[1]

Photochemical degradation is by far the most important process of natural removal of nitro-PAHs in the environment.[1] Consequently, the investigation of the excited states relaxation pathways is a necessary first step to understand its photochemical fate in the environment and to develop effective atmospheric pollution control strategies.

The orientation of the nitro group has been suggested to control the reaction rate, the formation of intermediates, and the products in nitro-PAH photochemistry.[1] This is generally known as the Chapman's orientation−photoreactivity relationship.[12] This relationship, widely used to explain nitro-PAHs photochemistry,[1] is primarily based on detailed mechanistic studies performed by Chapman and co-workers on 9-nitroanthracene in acetone solution in 1966.[12] It involves the formation of a nitro to nitrite transition state, whose probability of formation depends on the orientation of the nitro group relative to the aromatic rings of the PAH. Two types of mechanistic pathways have been considered for the nitro to nitrite rearrangement: (1) a dissociation−recombination mechanism and (2) an intramolecular rearrangement mechanism.[12] The latter transition state has been favored to explain the photochemistry of 9-nitroanthracene in acetone solution.[12] However, direct evidence supporting the validity and generality of Chapman's orientation−photoreactivity relationship not only is lacking but also is currently under debate.[13]

In this work, we combined femtosecond transient absorption spectroscopy with quantum chemical calculations to study the excited state dynamics of 1-nitropyrene (1NP) in detail. 1-Nitropyrene is among the most abundant nitro-PAHs detected in urban air, found at ng/m^3 concentrations.[14,15] It has been implicated to the direct-acting mutagenicity of diesel exhaust particles.[16–18] Its photodegradation results in at least nine primarily oxidation photoproducts.[19–22] Some of the quinone products might act as efficient photosensitizers[1,12,19,23–26] and thus have the potential for increased phototoxicity.

Our results show that 406 nm excitation of 1NP populates the Franck−Condon lowest singlet excited state with very small excess vibrational energy. Conformational relaxation of the lowest singlet excited state, primarily due to planarization of the nitro group relative to the pyrene aromatic rings, results in an ultrafast nonradiative decay to an almost isoenergetic $n\pi^*$ triplet state. The $n\pi^*$ triplet state internally converts to the lowest excited $\pi\pi^*$ triplet state, which decays to the ground state in 30 μs in hexane and cyclohexane solutions. The implications of this excited state deactivation mechanism to Chapman's orientation−photoreactivity relationship and to the photochemistry of 1NP are briefly discussed.

* Corresponding author. E-mail: carlos.crespo@case.edu.
† Case Western Reserve University.
‡ Adam Mickiewicz University.
§ University of Puerto Rico.

10.1021/jp803847q CCC: $40.75
Published on Web 06/21/2008

Experimental Section

Chemicals. 1-Nitropyrene was obtained from Sigma-Aldrich and was recrystallized three times from methanol to remove minor fluorescent impurities (mainly 1-hydroxypyrene). Hexane (Fluka Chemika for UV spectroscopy) and cyclohexane (B&J spectro grade) were used as received.

Steady State Absorption and Emission Measurements. Absorption spectra were measured using a UV−VIS-550 (JASCO) spectrophotometer in a 4 mm optical cell (Figure S1a). Emission spectra were recorded using a modified SPF-500 (Aminco-Bowman) spectrofluorometer with the single-photon counting detection. Emission and excitation slits of 5 mm were used (Figure S1b). The excitation wavelength was set at 406 nm and the solution absorbance was 0.6 in a 1 mm cell.

Transient Absorption Measurements. Ultrafast UV−vis broadband absorption measurements were performed using the home-built spectrometer described previously.[27] The laser system consists of a short pulse titanium-sapphire oscillator (Coherent, Mira) generating 30 fs pulses at 800 nm that seeds a high energy titanium-sapphire regenerative amplifier (Coherent/Positive Light, Legend HE USP). The regenerative amplifier produces 2.5 mJ, 40 fs pulses at 1 kHz. The main part of the beam is used to pump two OPAs (OPerA Coherent) equipped with UV−vis and SFG modules, respectively, allowing the generation of pump pulse tunable from 240 to 800 nm. A small portion of the fundamental is used for white light generation in the range 350−700 nm by focusing a small portion of the fundamental output (800 nm, 1.5 μJ) into a 1 mm thick CaF_2 plate. To create a stable white light continuum, the fundamental power density in the focus is carefully adjusted and each 3 s the CaF_2 rotates by a small angle of 1.5°. A 50 mm lens collimates the white light continuum beam, which then passes through an iris to select the central, uniform region of the beam profile. The white light continuum is split into two parts, probe and reference, of nearly equal intensity by using reflection from the front (probe) and back (reference) surfaces of a 6 mm thick CaF_2 plate. Both beams pass through the sample, but only the probe overlaps with the pump beam in the sample.

The absorbance of the sample solutions was typically 0.5 at the excitation wavelength (406 nm), and the sample volume was 50 mL. The sample was circulated in a Harrick Scientific flow cell (1 mm thick CaF_2 windows; optical path length 1 mm). The pump pulse energy was ~6 μJ at the sample position. The entire set of pump−probe delay positions (cycle) was repeated at least three times, to determine data reproducibility from cycle to cycle. Steady state absorption measurements before and after transient absorption experiments showed that photodegradation of 1NP were negligible under the experimental conditions used. To avoid rotational diffusion effects, the angle between polarizations of the pump beam and the probe beam was set to the magic angle (54.7°). Transient absorption spectra were corrected for chirp in the probe continuum.[28] The kinetic traces were analyzed by fitting to a sum of exponential terms, convoluted with a Gaussian response function in the global fitting procedure. The instrument response was 115 fs (fwhm). All experiments were performed at room temperature.

Nanosecond transient absorption experiments were performed using a spectrometer described previously.[29] Pump pulses (355 nm) with energies about 1 mJ, 8 ns (fwhm), were generated at a repetition rate of 0.5 Hz by a Q-switched Nd:YAG laser (Continuum Surelite II). The probing light source was a 150 W xenon arc lamp (Applied Photophysics), used in the pulsed mode with a 1 Hz repetition rate. The transmitted probe light was dispersed by a monochromator (6 nm spectral resolution, Acton Research SpectraPro 300i) and detected by a photomultiplier (R928 Hamamatsu) coupled to a digital oscilloscope (Tektronix TDS 680 C). A home-made program written in LabView 4.1 environment was used for the ΔA calculations, data fitting, and the dialog between the PC and the oscilloscope. An input output card (PCI-MIO-16XE-10) was used for time-control of TTL signals to trigger the laser, the lamp pulser, and the shutters. Experiments were performed on 4 mL solution samples contained in a quartz cell (1 cm × 1 cm section). All solutions were deaerated for about 15 min prior to each experiment with an argon gas flow to remove traces of O_2. A sample absorbance of about 1 at the laser excitation wavelength (355 nm) was generally used. This corresponds to a 1NP concentration of approximately 9×10^{-5} M.

Computational Methods

Ground and excited state calculations were performed using the Gaussian 03 suite of programs.[30] The following gradient procedures were used for ground state optimizations: HF/6-31G(d,p), HF/6-31++G(d,p), B3LYP/6-31G(d,p), and B3LYP/6-31++G(d,p) levels of theory.[31,32] DFT methods, in particular the B3LYP hybrid DFT method, have been shown to reproduce reliable ground state geometries.[33] It also require less time and computer resources than more accurate CASSF and CASSPT2 methods.[34]

Excited state optimizations were performed at the CIS level of theory using the following gradient procedures: CIS/3−21G, CIS/3-21G(d,p), CIS/6-31G, and CIS/6-31G(d,p) levels of theory. Vertical excited states calculations were performed at the TDDFT level of theory using the B3LYP and PBE1PBE functionals. Bulk solvent effects on the vertical excitation energies were studied by performing self-consistent reaction field (SCRF) calculations using the polarizable continuum model (PCM)[35] with the integral equation formalism (SCRF=IEFPCM)[36] on the gas phase optimized ground and excited state geometries. The default solvent parameters were used throughout the work.

Optimized ground and excited state geometries were calculated without any geometrical restriction, except those enforced by symmetry. All optimized geometries were confirmed to be stationary points through vibrational frequency analysis.

Results

Ground and Excited States Quantum Chemical Calculations. The chief aim of this section is to present the most important 1NP electronic structure properties of direct relevance to the interpretation of the experimental observations. Figure 1a shows the optimized ground state structure of 1NP in the gas phase at the B3LYP/6-31++G(d,p) level of theory. An inspection of the frequency calculations shows that this structure is a local minimum in the ground state potential energy surface. A nitro-aromatic torsion angle (defined on Figure 1a) of 27.46° is obtained for the fully optimized ground state structure. A torsional angle of 32.8° is predicted at the HF/6-31G(d,p) level (see nuclear coordinates in the Supporting Information). Semiempirical results obtained a nitro-aromatic torsion angle of 97.3° (at MNDO), 32.0° (at AM1), and 55.6° (at PM3).[13] Previous DFT calculations predicted a nitro-aromatic torsion angle of 23.15° at the B3LYP/6-31G* level of theory,[37] in good agreement with our calculations. Experimentally, ^{1}H-NMR, MS, and UV−vis spectroscopic techniques estimate a parallel orientation of the nitro group in 1NP.[13,38–40] In particular, MS experiments suggest a torsional angle of 30.0° for 1NP,[40] in very good agreement with our ground state DFT and HF calculations.

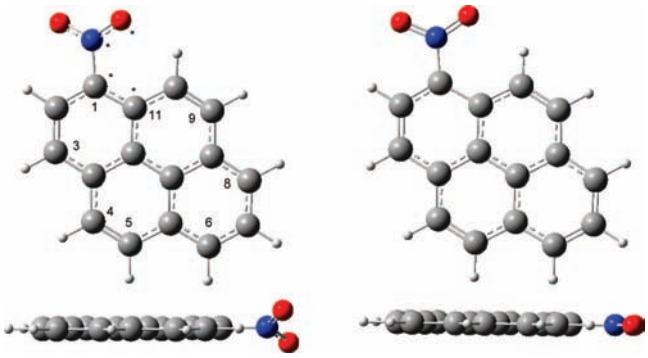

Figure 1. Optimized 1NP geometries: (a) ground state at B3LYP/6-31++G(d,p) and (b) first singlet excited state at CIS/6-31G(d,p) levels of theory. The optimized ground state nuclear coordinates of 1NP at HF/6-31G(d,p) level of theory are given as Supporting Information (see text). Numbering and nitro-aromatic torsional angle, highlighted with asterisks, are shown in Figure 1a.

TABLE 1: 1NP Vertical Excitation Energies at TDDFT/6-31++G(d,p)

	E (eV)[a]		E (eV)[b,c]	
state	B3LYP	PBE1PBE	B3LYP	PBE1PBE
$T_1(\pi\pi^*)$	1.90	1.81		
	652.51 nm	683.38 nm		
$T_2(n\pi^*)$	2.85	2.71		
$T_3(n\pi^*)$	2.98	3.00		
$S_1(\pi\pi^*)$	2.99	3.12	2.80	2.89
	414.7 nm	397.2 nm	443.2 nm	429.2 nm
	(0.2893)[d]	(0.3160)	(0.5592)	(0.5898)
ΔE_g[e]	0.01	0.12		

[a] Using ground state optimized geometry in gas phase at B3LYP/6-31++G(d,p) level of theory. [b] IEFPCM in the presence of cyclohexane dielectric continuum. [c] Predicted fluorescence emission using the optimized lowest excited singlet state geometry at the CIS/6-31G(d,p) level of theory. [d] Oscillator strength in parentheses. [e] $\Delta E_g = E(S_1) - E(T_3)$.

The fully optimized geometry of the lowest excited singlet state of 1NP in the gas phase is shown in Figure 1b at the CIS/6-31G(d,p) level of theory. Almost identical optimized nuclear coordinates were obtained using a smaller basis set (CIS/6-31G). The eigenvalues from frequency calculations are all real at the CIS/6-31G level of theory, showing that the excited state geometry is a local minimum in the S_1 potential energy surface. The most evident conformational change is the rotation of the nitro group from 32.8° in the ground state to a nitro-aromatic torsional angle of 0.07° in the lowest excited singlet state at HF/6-31G(d,p) at CIS/6-31G(d,p) levels of theory, respectively. Visual inspection of Figure 1 shows that several bond lengths change in the S_1 state relative to the ground state. A comparison of the S_1 optimized geometry with that optimized in the ground state at HF/6-31G(d,p) level predicts that the C1−N bond stretches by 0.037 Å, and the C1−C2, C1−C11, and N−O bonds elongate by 0.014, 0.053, and 0.014 Å, respectively. A similar bond length trend is predicted using the DFT ground state geometry (Figure 1).

Vertical excitation energies were also obtained at the TDDFT level of theory for the optimized ground and lowest excited singlet state structures using the B3LYP and PBE1PBE functionals (Table 1). Calculations were performed in the gas phase and in the presence of a dielectric continuum (IEFPCM) using the PBE1PBE functional with the 6-31++G(d,p) standard basis set. This functional has been shown to reproduce satisfactorily the absorption and emission spectra of organic heteroatomic molecules when bulk solvent effects are included.[41] In this work, cyclohexane was chosen to model the bulk solvent effects on the vertical excited states energies of 1NP.

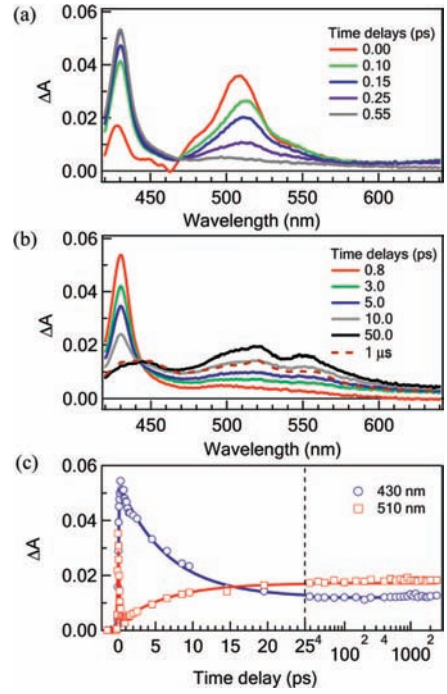

Figure 2. Transient absorption spectra for 1NP in hexane after photoexcitation at 406 nm: (a) first 0.55 ps; (b) from 0.8 to 50 ps. (c) Transient decay signals at 430 and 510 nm probe wavelengths. The TA spectrum at 0 ps delay time around 460 nm is slightly distorted by a not fully subtracted stimulated Raman signal from the solvent (2886 cm^{-1} CH stretching). Figure 2b shows the triplet−triplet absorption spectrum (broken line) of 1NP from nanosecond-transient absorption experiments at 1 μs delay time.

Table 1 shows singlet and triplet vertical excitation energies in the gas phase and in cyclohexane obtained using the optimized ground state structure. The lowest excited singlet and triplet (T_1) states are stabilized in the presence of solvent, and the second (T_2) and third (T_3) excited triplet states destabilized or stay unchanged, respectively (not shown). An inspection of the molecular orbitals and transition coefficients show that S_1 and T_1 states have primarily $\pi\pi^*$ character, and T_2 and T_3 states have mainly $n\pi^*$ character. The predicted absorption (~410 nm) and emission (~440 nm) energies (Table 1) are in very good agreement with the experimental absorption and emission spectra of 1NP in cyclohexane and hexane solutions (see Figure 1S). These results further support the accuracy of the calculations presented in this work.

The most important result is the prediction a small energy gap (0.01−0.12 eV) between S_1 and the T_3 states (Table 1). The small energy gap and the different electronic character of the S_1 and T_3 states, suggests a large spin-orbit coupling and an efficient singlet-triplet intersystem crossing for 1NP in nonpolar solvents.

Femtosecond Pump−Probe Transient Absorption Experiments. The femtosecond broadband transient absorption spectra of 1NP in hexane and cyclohexane are shown in Figures 2 and 3, respectively. The 1NP solutions were excited at 406 nm and probed with a white-light continuum pulse. The spectra were recorded from 420 to 650 nm. The transient absorption spectra feature positives bands in this spectral region and show changes in intensity and spectral peak position with respect to delay time. No indication of changes in bandwidths with time was observed.

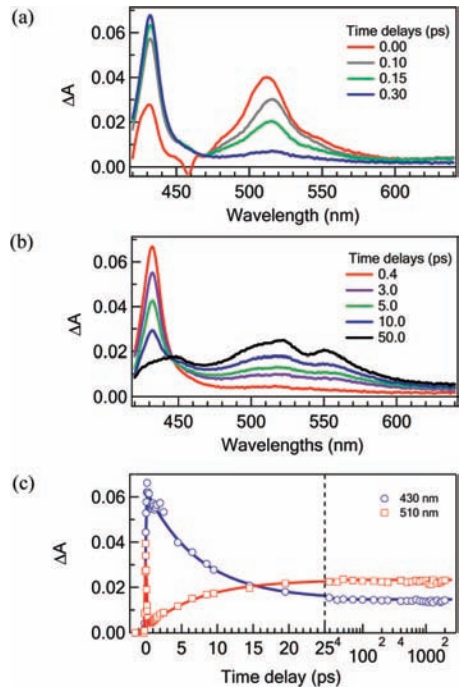

Figure 3. Transient absorption spectra for 1NP in cyclohexane after photoexcitation at 406 nm: (a) first 0.30 ps; (b) from 0.4 to 50 ps. (c) Transient decay signals at 430 and 510 nm probe wavelengths. The TA spectrum at 0 ps delay time around 460 nm is slightly distorted by a not fully subtracted stimulated Raman signal from the solvent.

TABLE 2: Excited State Lifetimes ($\pm 2\delta$) of 1NP in Two Different Solvents[a]

solvent	τ_1 (fs)	τ_2 (ps)
hexane	115 ± 16	7.2 ± 0.6
cyclohexane	79 ± 16	7.7 ± 0.4

[a] Global fit results at 430, 510, and 550 nm probe wavelengths (IRF = 115 fs; see Experimental Section for details.

SCHEME 1: Proposed Excited State Relaxation Mechanism for 1NP in Nonpolar Solvents[a]

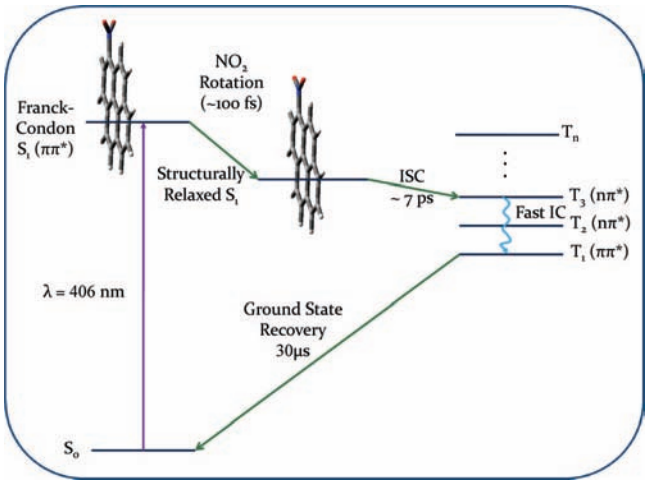

[a] Ultrafast fluorescence emission and internal conversion from the S_1 state are not shown (see text for details).

Table 2 shows the excited state lifetimes of 1NP in both solvents. These time constants were obtained by global fitting the decay signals at 430, 510, and 550 nm probe wavelengths. As can be observed from Figures 2 and 3, the spectral evolution and kinetics of 1NP are nearly the same in these two solvents within experimental uncertainties.

In the first 500 fs (Figures 2a and 3a), the 1NP transient absorption band with a maximum around 508 nm decays simultaneously with a 5 nm red shift (in hexane), whereas an increase of the transient absorption band with maximum around 430 nm is observed. This transformation is characterized by the presence of an isosbestic point around 470 nm. From 800 fs to 1.75 ps, the transient absorption spectra do not show any change in amplitude or band shape within experimental uncertainties and are characterized by an absorption band with maximum around 430 nm. From 1.75 to 50 ps, the transient absorption band with maximum at 430 nm decays and a transient spectrum showing three absorption band maxima at 440, 520, and 550 nm is formed.[42] The changes in transient absorption during this time interval are accompanied by the formation of an isosbestic point at 445 nm. No further changes in the transient absorption spectra are observed at delay times from 50 ps to 3 ns in hexane or cyclohexane solutions. Figures 2c and 3c show the decay signals at the 430 and 510 nm probe wavelengths. The decay signals in each solvent were globally fit to two exponential terms and a constant (Table 2). The constant offset is due to the formation of a transient species, which does not decay within our limited time window of 3 ns. Similar time constants observed at other probe wavelengths are not shown.

Discussion

Assignment of the Transient Absorption Signals. The femtosecond transient absorption spectra of 1NP in hexane and cyclohexane solutions show the presence of at least three different species in the spectral region from 420 to 650 nm (Figures 2 and 3). Our calculations suggest that excitation of 1NP at 406 nm populates the S_1 state with a small excess of vibrational energy. Consequently, the first transient absorption species is assigned to the Franck−Condon $S_1(\pi\pi^*)$ state. It has absorption maxima around 430 and 510 nm and decays within ~100 fs to form a species with absorption maximum at 430 nm. The latter is assigned to the relaxed S_1 state (i.e., $S_n \leftarrow S_1$ transition). It is formed by conformational relaxation of the S_1 state; i.e., the vertically excited S_1 state relaxes via a change in conformation along certain nuclear coordinates to reach the optimum S_1 equilibrium minimum. The presence of an isosbestic point at 470 nm supports this interpretation. The spectral shift observed during the first 500 fs is suggested to originate from a change in the Franck−Condon overlap between the S_1 and S_n states as the nuclear coordinates evolves. The major relaxation coordinate in the S_1 state is rotation of the nitro group from a ground state torsional angle of 32.8° to 0.07° in the lowest excited singlet state at the HF/6-31G(d,p) and CIS/6-31G(d,p) levels of theory, respectively (Figure 1). This conformational relaxation in the S_1 state occurs within the time resolution of our instrument in hexane and cyclohexane solutions (Table 2).

Our results show that the relaxed lowest excited singlet state decays to form a long-lived species with absorption maxima at 445, 520, and 550 nm. The time constant associated with this decay is 7 ps. The new species is assigned to the lowest T_1 state of 1NP ($T_n \leftarrow T_1$ transition), because it is identical to the triplet−triplet absorption spectrum of 1NP in hexane, recorded 1 μs after excitation using a nanosecond transient absorption setup (Figure 2b). The presence of an isosbestic point at 445 nm further supports this assignment. Our calculations show that the T_1 state of 1NP has a $\pi\pi^*$ character, in agreement with recent nanosecond transient absorption experiments of 1NP in different solvents.[43] The T_1 state has a lifetime of 30 μs in hexane, explaining its negligible decay within the time window of our instrument (3 ns).

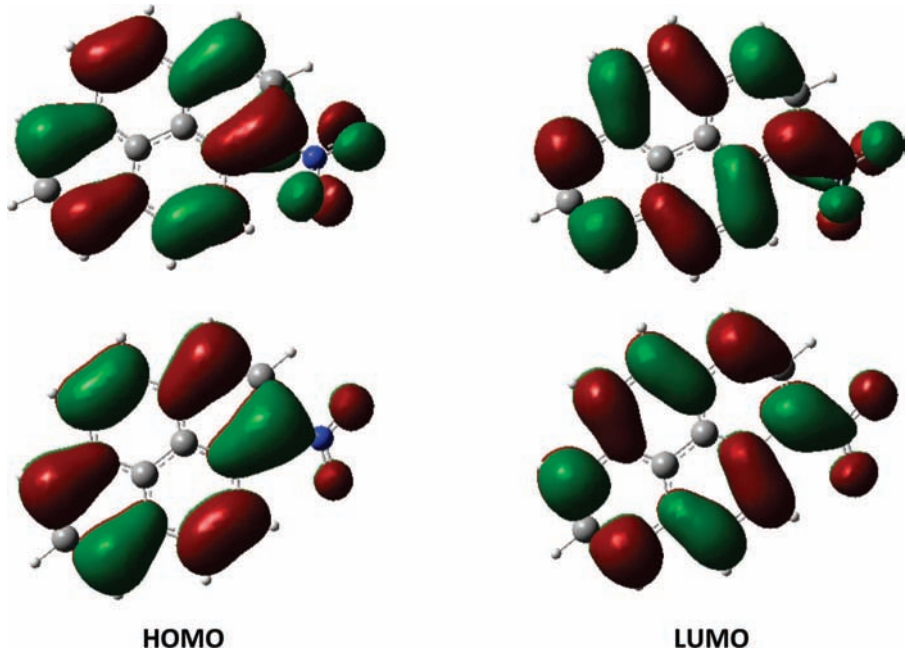

Figure 4. Frontier molecular orbitals: HOMO to LUMO transition accounts for 73% of the excitation coefficients in the vertical excitation (upper panel) and for 79% in the optimized (lower panel) lowest excited singlet state, respectively. The molecular orbitals were drawn using an isovalue of 0.02 au. The electron density of the nitro group is noticeably larger in the LUMO than in the HOMO, suggesting a partial charge transfer character in the lowest singlet excited state of 1NP.

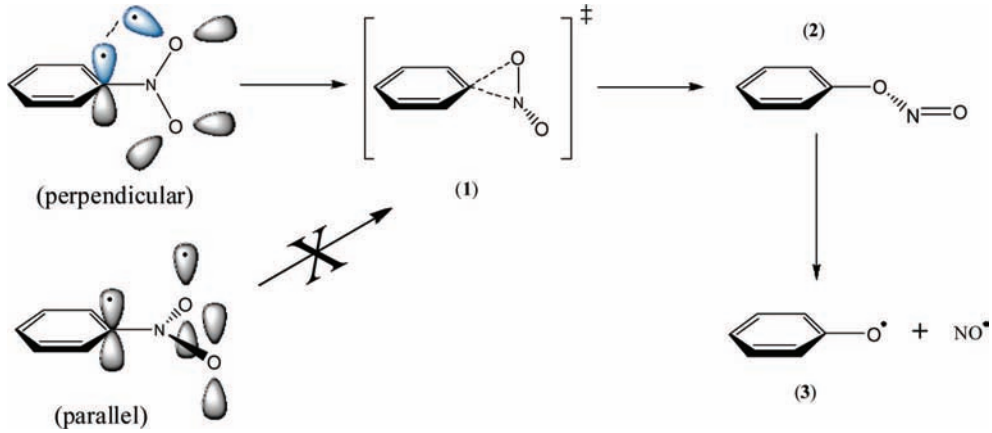

Figure 5. Schematic representation of Chapman's orientation−photoreactivity relationship in the photochemistry of nitro-PAHs.

The femtosecond transient absorption experiment shows that the singlet−triplet intersystem crossing (ISC) in 1NP occurs in ultrafast time scales. This result is in very good agreement with recent femtosecond up-conversion experiments for 1NP in polar solvents.[44] It is known that nitro-aromatic compounds undergo highly efficient ISC in the vapor phase.[45] In condensed phase, a 0.6 triplet yield has been measured for 1NP.[43,46] Thus, taking into consideration that 1NP is photoreactive (see below), ultrafast internal conversion from the excited singlet state to the ground state should not play a major (< 0.4) in the excited state relaxation of 1NP in hexane and cyclohexane solvents. Our calculations show that there are three excited triplet states below the S_1 state and predict that T_2 and T_3 states have mainly $n\pi^*$ character (Table 1). The T_3 state is almost isoenergetic to the S_1 state with an energy gap between 0.01 to 0.12 eV. Consequently, the ultrafast ISC in 1NP can be rationalized by the energy gap law[47,48] and an efficient one-center overlap between the $S_1(\pi\pi^*)$ and $T_3(n\pi^*)$ states.[49] The calculations suggest that there is a large spin-orbit coupling between S_1 and T_3 states leading to an ultrafast ISC lifetime in 1NP. Our results cannot rule out an involvement of the T_2 state in the singlet-triplet ISC process. Apparently, internal conversion from T_3 (and/or T_2) to T_1 is very fast (as expected); thus the instantaneous concentration of T_2/T_3 state is very low, or their transition cross sections in absorption are too small to be detected in our experiments.

Kinetic Model. The excited states relaxation mechanism that emerges from this combined experimental and computational study is summarized in Scheme 1: (1) Conformational relaxation of the Franck−Condon S_1 state to the relaxed S_1 state occurs primarily by conformational relaxation of the nitro-group. A molecular orbital analysis shows that this state has a moderate charge transfer character (Figure 4), likely because of the electron withdrawing properties of the nitro group. (2) Conformational relaxation in the S_1 manifold is followed by an efficient ISC to the T_3 (and/or T_2) state. (3) This, in turn, is followed by ultrafast internal conversion to the T_1 state with a triplet yield of $\sim$0.6,[43,46] which decays back to the ground state in $\sim$30 μs. From the triplet yield value we can estimate that less than 40% of the molecules in the S_1 state undergo internal conversion to the ground state. Our kinetic model is consistent with the double-exponential decay of 1NP of the lowest singlet state observed

by Peon and co-workers recently in methanol and 1-butanol using the femtosecond-fluorescence up-conversion technique.[44]

Implications to 1NP Photochemistry. The photochemistry of nitro-PAHs has been proposed to be controlled by the orientation of the nitro group relative to the aromatic plane.[1,12] On the one hand, rearrangement of the nitro group to a nitrite intermediate is proposed to be the first step after excitation for perpendicular nitro group orientations (Figure 5). On the other, the parallel orientation of the nitro group is unfavorable for the orbital overlap in the excited state, precluding the formation of the oxaziridine-type transition state (Figure 5). The prevalent hypothesis is that at perpendicular orientations, there is an increased probability of overlap between the half-vacant, nonbonding orbital of the nitro group and the adjacent orbital of the aromatic moiety in the excited state.[12] This orbital overlap leads to the formation of an oxaziridine-type transition state (**1**) that could collapse to the nitrite intermediate (**2**). A dissociation reaction then generates nitrogen oxide and aryloxy radicals (**3**). Our calculations predict that the nitro group in 1NP is almost parallel to the aromatic moiety in the relaxed S_1 state. No evidence of a nitro-to-nitrite transition state was found in our experiments, in line with the parallel orientation of the nitro group obtained in our calculations and with Chapman's relationship.

Interestingly, nitro-PAHs with parallel nitro groups show higher mutagenic activity than those with perpendicular orientations.[50–52] In addition, their photochemistry is more complex due to the formation of many different photoproducts.[1] In particular, 1-hydroxypyrene (1HOP) is one of the major product in the photochemistry of 1NP, formed in a 10^{-4} yield in cyclohexane solutions.[1,43] This suggests that the pyrenyloxyl radical should be formed, followed by hydrogen atom abstraction from the solvent to form 1HOP.[43] A nitro−nitrite transition state has been suggested as potential precursor of the pyrenyloxyl radical (Figure 5).[12,53–55] However, our computational results suggest that the nitro group is almost parallel to the pyrene moiety in the S_1 state. This nitro group orientation is not expected to favor an intramolecular nitro to nitrite rearrangement to form the pyrenyloxyl radical (see Figure 5). The pyrenyloxyl radical might be partially form from an excited triplet state of 1NP.[12,43]

An alternative pathway proposed by Chapman[12] and others[56] involve a dissociation−recombination mechanism, where the C−N bond is weakened in the excited singlet state leading to a pyrenyl (P$^{\bullet}$) and nitrogen(IV) dioxide geminate radical pair. This radical pair is suggested to rearrange to a nitrite intermediate, which then form the pyrenyloxyl radical. The partial charge transfer character of the lowest excited singlet state predicted in our calculations (Figure 4) seems to support the dissociation−recombination mechanism. However, our experimental results do not provide direct evidence for any of these transient absorption species to explain the formation of 1HOP in cyclohexane solutions. It is likely that these transient absorption species maybe formed in very low yield or have small transition cross sections in absorption to be detected in our experiments. Clearly, much work is needed before Chapman's orientation−reactivity relationship can be generalized and the photochemical fate of nitro-PAHs in the environment could be fully understood.

Conclusions

A combined experimental and computation study on the excited state dynamics of 1NP in hexane and cyclohexane solutions is presented. It is shown that excitation of 1NP to its lowest $\pi\pi^*$ excited singlet state results in an approximately 100 fs conformational relaxation to the singlet state minimum in hexane and cyclohexane solutions. The primary nuclear coordinate associate with this conformational dynamics is the rotation of the nitro group from 32.8° in the ground state to 0.07° in the excited singlet state minimum. The small energy gap between this $\pi\pi^*$ singlet state and a high-energy $n\pi^*$ triplet state results in an efficient spin-orbit coupling with a 1.4×10^{11} s^{-1} ISC rate constant. The $n\pi^*$ triplet state internally convert in ultrafast time scales to the lowest $\pi\pi^*$ excited triplet state, which decays back to the ground state in 30 μs in hexane. It is shown in this work that femtosecond broadband transient absorption spectroscopy in combination with computational methods can be used as effective diagnostic tools to understand at the molecular level the excited state dynamics and photochemistry of environmentally relevant compounds.

Acknowledgment. C.E.C.H. and G.B. thank Professor Terry L. Gustafson and The Ohio State University Center for Chemical and Biophysical Dynamics for donation of laser time to perform some of the experiments presented in this work. Stationary absorption and nanosecond transient absorption spectra were recorded at Adam Mickiewicz University. C.E.C.H. thanks the Ohio State Supercomputer Center for generous allotment of computer time and the financial support from the National Science Foundation, Academic Careers in Engineering and Science (NSF ACES) Program and from NSF-MRI Grant CHE0443570. R.A. acknowledges the financial support from NIH-SCORE Grant 5S-06GM08102.

Supporting Information Available: Steady state absorption and emission spectra of 1-nitropyrene in nonpolar solvents and ground and lowest singlet excited state optimized nuclear coordinates at HF and DFT levels of theory. This material is available free of charge via the Internet at http://pubs.acs.org.

References and Notes

(1) Yu, H. *J. Environ. Sci. Health C* **2002**, *C20*, 149.
(2) Arlt, V. M. *Mutagenesis* **2005**, *20*, 399.
(3) Tokiwa, H.; Ohnishi, Y. *CRC Crit. Rev. Toxicol.* **1986**, *17*, 23.
(4) Möller, L. *Environ. Health Perspect.* **1994**, *102*, 139.
(5) Purohit, V.; Basu, A. K. *Chem. Res. Toxicol.* **2000**, *13*, 673.
(6) Christensen, H. C. *J. Phys. Chem.* **1973**, *77*, 983.
(7) Diesel and Gasoline Engine Exhausts and Some Nitroarenes. In *IARC Monographs on the Evaluation of Carcinogenic Risks to Humans*; World Health Organization, International Agency for Research on Cancer; Lyon, France, 1989; No. 46.
(8) Finlayson-Pitts, B. J.; Pitts, J. N. *Science* **1997**, *276*, 1045.
(9) Atkinson, R.; Arey, J. *Environ. Health Perspect.* **1994**, *102*, 117.
(10) Arey, J. Atmospheric Reactions of PAHs Including Formation of Nitroarenes. In *PAHs and Related Compounds*; Neison, A. H., Ed.; Springer-Verlag: Berlin, Germany, 1998; p 347.
(11) Arey, J.; Atkinson, R. Photochemical Reactions of PAHs in the Atmosphere. In *PAHs: An Ecotoxicological Perspective*; Douben, P. E. T., Ed.; John Wiley & Sons: Chichester, England, 2003; p 47.
(12) Chapman, O. L.; Heckert, D. C.; Reasoner, J. W.; Thackaberry, S. P. *J. Am. Chem. Soc.* **1966**, *88*, 5550.
(13) Warner, S. D.; Farant, J.-P.; Butler, I. S. *Chemosphere* **2004**, *54*, 1207.
(14) Arey, J.; Zielinska, B.; Atkinson, R.; Winer, A. M. *Mutat. Res.* **1988**, *207*, 45.
(15) Hayakawa, K.; Murahashi, T.; Butoh, M.; Miyazaki, M. *Environ. Sci. Technol.* **1995**, *29*, 928.
(16) Hayakawa, K.; Nakamura, A.; Terai, N.; Kizu, R.; Ando, K. *Chem. Pharm. Bull.* **1997**, *45*, 1820.
(17) Salmeen, I.; Durisin, A. M.; Prater, T. J.; Riley, T. *Mutat. Res.* **1982**, *104*, 17.
(18) Kawanaka, Y.; Sakamoto, K.; Wang, N.; Yun, S.-J. *J. Chromatogr. A* **2007**, *1163*, 312.
(19) Holloway, M. P.; Biaglow, M. C.; McCoy, E. C.; Anders, M.; Rosenkranz, H. S.; Howard, P. C. *Mutat. Res.* **1987**, *187*, 199.
(20) Yang, D. T. C.; Chou, A.; Chen, E.; Chiu, L.-H.; Ni, Y. *Polycycl. Arom. Compd.* **1994**, *5*, 201.

(21) Yasahara, A.; Huwa, K. *Chem. Lett. (Jpn.)* **1983**, 347.
(22) Koizumi, A.; Suzuki, T.; Saitoh, N.; Kamiyama, S. A. *Arch. Environ. Health* **1994**, *49*, 87.
(23) Pitts, J. N.; van Cauwenberghe, K. A.; Grosjean, D.; Schmid, J. P.; Fitz, D. R.; Belser, W. L.; Knudson, G. B.; Hynds, P. M. *Science* **1978**, *202*, 515.
(24) Stark, G.; Stauff, J.; Miltenburger, H. G.; Stumm-Fischer, I. *Mutat. Res.* **1985**, *155*, 27.
(25) Ioki, Y. *J. Chem. Soc., Perkin Trans. 2* **1977**, 1240.
(26) Fukuhara, K.; Kurihara, M.; Miyata, N. *J. Am. Chem. Soc.* **2001**, *123*, 8662.
(27) Burdzinski, G.; Hackett, J. C.; Wang, J.; Gustafson, T. L.; Hadad, C. M.; Platz, M. S. *J. Am. Chem. Soc.* **2006**, *128*, 13402.
(28) Nakayama, T.; Amijima, Y.; Ibuki, K.; Hamanoue, K. *Rev. Sci. Instrum.* **1997**, *68*, 4364.
(29) Burdzinski, G.; Maciejewski, A.; Buntinx, G.; Poizat, O.; Lefumeux, C. *Chem. Phys. Lett.* **2004**, *384*, 332.
(30) Frisch, M. J.; Trucks, G. W.; Schlegel, H. B.; Scuseria, G. E.; Robb, M. A.; Cheeseman, J. R.; Zakrzewski, V. G.; Montgomery, J. A., Jr.; Stratmann, R. E.; Burant, J. C.; Dapprich, S.; Millam, J. M.; Daniels, K. N.; Kudin, K. N.; Strain, M. C.; Farkas, O.; Tomasi, J.; Barone, V.; Cossi, M.; Cammi, R.; Mennucci, B.; Pomelli, C.; Adamo, C.; Clifford, S.; Ochterski, J.; Petersson, G. A.; Ayala, P. Y.; Cui, Q.; Morokuma, K.; Malick, D. K.; Rabuck, A. D.; Raghavachari, K.; Foresman, J. B.; Cioslowski, J.; Ortiz, J. V.; Baboul, A. G.; Stefanov, B. B.; Liu, G.; Liashenko, A.; Piskorz, P.; Komaromi, I.; Gomperts, R.; Martin, R. L.; Fox, D. J.; Keith, T.; Al-Laham, M. A.; Peng, C. Y.; Nanayakkara, A.; Gonzalez, C.; Challacombe, M.; Gill, P. M. W.; Johnson, B. G.; Chen, W.; Wong, M. W.; Andres, J. L.; Head-Gordon, M.; Replogle, E. S.; Pople, J. A. Gaussian 03, revision D.01; Gaussian, Inc.: Wallingford, CT, 2004.
(31) Becke, A. D. *J. Chem. Phys.* **1993**, *98*, 1372.
(32) Lee, C.; Yang, W.; Parr, R. G. *Phys. Rev.* **1988**, *B37*, 785.
(33) Momany, E. A.; Willett, J. L. *J. Comput. Chem.* **2000**, *21*, 1204.
(34) Cramer, C. J. *Essentials of computational chemistry: theories and models*; John Wiley & Sons: New York, 2002.
(35) Barone, V.; Cossi, M.; Tomasi, J. *J. Chem. Phys.* **1997**, *107*, 3210.
(36) Cances, E.; Mennucci, B.; Tomasi, J. *J. Chem. Phys.* **1997**, *107*, 3032.
(37) Onchoke, K. K.; Hadad, C. M.; Dutta, P. K. *Polycycl. Arom. Compd.* **2004**, *24*, 37.
(38) Jung, H.; Shaikh, A. U.; Heflich, R. H.; Fu, P. P. *Environ. Mol. Mutagen.* **1991**, *17*, 169.
(39) Miller, D. W.; Evans, F. E.; Fu, P. P. *Spectrosc. Int. J.* **1985**, *4*, 91.
(40) Lin, S.-T.; Jih, Y.-F.; Fu, P. P. *J. Org. Chem.* **1996**, *61*, 5271.
(41) Improta, R.; Barone, V.; Santoro, F. *J. Phys. Chem. B* **2007**, *111*, 14080.
(42) Note that the transient absorption spectra might be affected by stimulated emission (negative signal), particularly around 450 nm where the weak stationary emission of 1NP peaks (see steady state emission spectrum of 1NP in the Supporting Information).
(43) Arce, R.; Pino, E. F.; Valle, C.; Ágreda, J. *J. Phys. Chem. A*, submitted for publication.
(44) Morales-Cueto, R.; Esquivelzeta-Rabell, M.; Saucedo-Zugazagoitia, J.; Peon, J. *J. Phys. Chem. A* **2007**, *111*, 552.
(45) Kasha, M. *Radiat. Res. Suppl.* **1960**, *2*, 243.
(46) Scheerer, R.; Henglein, A. *Ber. Bunsen-Ges.* **1977**, *81*, 1234.
(47) Lim, E. C. *J. Phys. Chem.* **1986**, *90*, 6770.
(48) El-Sayed, M. A. *J. Chem. Phys.* **1962**, *36*, 573.
(49) El-Sayed, M. A. *J. Chem. Phys.* **1963**, *38*, 2834.
(50) Fu, P. P.; Chou, M. W.; Beland, F. A. *Effects of nitro substitution on the in vitro metabolic activation of polycyclic aromatic hydrocarbons*; CRC Press: Boca Raton, FL, 1988; Vol. II.
(51) Fu, P. P.; Herrero-Saenz, D. *Environ. Carcinog. Ecotox. Rev.* **1999**, *C17*, 1.
(52) Fu, P. P. *Drug Metabolism Rev.* **1990**, *22*, 209.
(53) He, Y.; Gahlmann, A.; Feenstra, J. S.; Park, S. T.; Zewail, A. H. *Chem. Asian. J.* **2006**, *1*−*2*, 56.
(54) Hamanoue, K.; Nakayama, T.; Ushida, K.; Kajiwara, K.; Yamanaka, S. *J. Chem. Soc., Faraday Trans.* **1991**, *87*, 3365.
(55) Hamanoue, K.; Nakayama, T.; Kajiwara, K.; Yamanaka, S. *J. Chem. Soc., Faraday Trans.* **1992**, *88*, 3145.
(56) Brown, H. W.; Pimentel, G. C. *J. Chem. Phys.* **1958**, *29*, 883.

JP803847Q